Inducers of the endothelial cell barrier identified through chemogenomic screening in genome-edited hPSC-endothelial cells

Filip Roudnicky[a,1], Jitao David Zhang (张继涛)[b,1,2], Bo Kyoung Kim[c], Nikhil J. Pandya[b], Yanjun Lan[a], Lisa Sach-Peltason[d], Heloise Ragelle[c], Pamela Strassburger[c], Sabine Gruener[c], Mirjana Lazendic[c], Sabine Uhles[c], Franco Revelant[c], Oliv Eidam[d], Gregor Sturm[b], Verena Kueppers[c], Klaus Christensen[a], Leonard D. Goldstein[e], Manuel Tzouros[b], Balazs Banfai[b], Zora Modrusan[e], Martin Graf[a], Christoph Patsch[a], Mark Burcin[a], Claas A. Meyer[a,3], Peter D. Westenskow[c,2,3], and Chad A. Cowan[f,g,h,2,3]

[a]Therapeutic Modalities, Pharmaceutical Research and Early Development, Roche Innovation Center Basel, F. Hoffmann-La Roche Ltd., CH-4070 Basel, Switzerland; [b]Pharmaceutical Sciences, Pharmaceutical Research and Early Development, Roche Innovation Center Basel, F. Hoffmann-La Roche Ltd., CH-4070 Basel, Switzerland; [c]Ocular Technologies, Immunology, Infectious Diseases and Ophthalmology, Pharmaceutical Research and Early Development, Roche Innovation Center Basel, F. Hoffmann-La Roche Ltd., CH-4070 Basel, Switzerland; [d]Pharma Research and Early Development Informatics, Pharmaceutical Research and Early Development, Roche Innovation Center Basel, F. Hoffmann-La Roche Ltd., CH-4070 Basel, Switzerland; [e]Molecular Biology Department, Genentech Inc., South San Francisco, CA 94080; [f]Division of Cardiology, Department of Medicine, Beth Israel Deaconess Medical Center, Harvard Medical School, Boston, MA 02215; [g]Department of Stem Cell and Regenerative Biology, Harvard University, Cambridge, MA 02138; and [h]Harvard Stem Cell Institute, Harvard University, Cambridge, MA 02138

Edited by Christer Betsholtz, Uppsala University, Uppsala, Sweden, and accepted by Editorial Board Member Rakesh K. Jain May 26, 2020 (received for review July 5, 2019)

The blood–retina barrier and blood–brain barrier (BRB/BBB) are selective and semipermeable and are critical for supporting and protecting central nervous system (CNS)-resident cells. Endothelial cells (ECs) within the BRB/BBB are tightly coupled, express high levels of Claudin-5 (CLDN5), a junctional protein that stabilizes ECs, and are important for proper neuronal function. To identify novel CLDN5 regulators (and ultimately EC stabilizers), we generated a CLDN5-P2A-GFP stable cell line from human pluripotent stem cells (hPSCs), directed their differentiation to ECs (CLDN5-GFP hPSC-ECs), and performed flow cytometry-based chemogenomic library screening to measure GFP expression as a surrogate reporter of barrier integrity. Using this approach, we identified 62 unique compounds that activated CLDN5-GFP. Among them were TGF-β pathway inhibitors, including RepSox. When applied to hPSC-ECs, primary brain ECs, and retinal ECs, RepSox strongly elevated barrier resistance (transendothelial electrical resistance), reduced paracellular permeability (fluorescein isothiocyanate-dextran), and prevented vascular endothelial growth factor A (VEGFA)-induced barrier breakdown in vitro. RepSox also altered vascular patterning in the mouse retina during development when delivered exogenously. To determine the mechanism of action of RepSox, we performed kinome-, transcriptome-, and proteome-profiling and discovered that RepSox inhibited TGF-β, VEGFA, and inflammatory gene networks. In addition, RepSox not only activated vascular-stabilizing and barrier-establishing Notch and Wnt pathways, but also induced expression of important tight junctions and transporters. Taken together, our data suggest that inhibiting multiple pathways by selected individual small molecules, such as RepSox, may be an effective strategy for the development of better BRB/BBB models and novel EC barrier-inducing therapeutics.

CLDN5 | human pluripotent stem cell-derived endothelial cells | endothelial cell barrier | genome editing | chemogenomic library

Central nervous system endothelial cells (CNS-ECs) are highly specialized and critical for CNS homeostasis (1, 2). Blood–retinal barrier and blood–brain barrier (BRB/BBB) breakdown is implicated in multiple common retinal and neurological diseases, including, but not limited to, age-related macular degeneration, diabetic retinopathy (3), Alzheimer's disease, Parkinson's disease, and Huntington's disease. Understanding how BRB/BBB is generated and maintained could be useful for generating more relevant cellular models for drug discovery, and for developing novel therapies for the diseases listed above and others (4).

Dynamic control over a specialized set of dynamically regulated tight cell–cell junction proteins (5) is required to generate and maintain BRB/BBB. Of all of the known CNS-EC junctional proteins, Claudin-5 (CLDN5) (6) might be the most important based on gene-profiling and loss-of-function analyses. Besides being the most highly expressed tight junction gene in CNS-derived ECs (Fig. 1*A*), it is the most abundantly expressed genes in CNS-ECs (7, 8). *Cldn5* global knock-out mice exhibit excessive vascular permeability in the brain and therefore die shortly after birth (9). Excessive vascular permeability in different brain regions was also observed in these mice after small interfering RNA-mediated *Cldn5* ablation (10) or inducible EC-specific ablation with result in schizophrenia-like phenotypes (11). Understanding how Claudin-5 and other important CNS-EC proteins are regulated in CNS-ECs is challenging because CNS-ECs are difficult to isolate and manipulate, and the ECs quickly lose their hallmark barrier properties when cultured (12). Developing a more relevant BRB/BBB model to address this unmet need and to support therapeutic target discovery is the focus of this study.

Author contributions: F. Roudnicky, J.D.Z., P.D.W., and C.A.C. designed research; F. Roudnicky, B.K.K., N.J.P., H.R., P.S., S.G., M.L., K.C., M.G., C.P., M.B., and C.A.M. performed research; F. Roudnicky, M.T., and Z.M. contributed new reagents/analytic tools; F. Roudnicky, J.D.Z., B.K.K., N.J.P., Y.L., L.S.-P., S.U., F. Revelant, O.E., G.S., V.K., L.D.G., and B.B. analyzed data; F. Roudnicky, J.D.Z., and B.K.K. wrote the paper; F. Roudnicky, J.D.Z., P.D.W., and C.A.C. conceived the study; F. Roudnicky, J.D.Z., and P.D.W. guided the research; and B.K.K., N.J.P., Y.L., and V.K. performed experiments.

Competing interest statement: This study is supported by F. Hoffmann-La Roche Ltd. F. Roudnicky, J.D.Z., B.K.K., N.J.P., Y.L., L.S.-P., H.R., P.S., S.G., M.L., S.U., F. Revelant, O.E., G.S., V.K., K.C., M.T., B.B., M.G., C.P., M.B., C.A.M., and P.D.W. are employees of F. Hoffmann-La Roche. L.D.G. and Z.M. are employees of Genentech Inc. F. Roudnicky, N.J.P., and V.K. were supported by a Roche postdoctoral fellowship. B.K.K. was supported by a Roche doctoral fellowship. C.A.C. is a founder and chief scientific officer of Sana Biotechnology. Neither a reagent nor any funding from Sana Biotechnology was used in this study.

This article is a PNAS Direct Submission. C.B. is a guest editor invited by the Editorial Board.

Data deposition: Data are available at Gene Expression Omnibus (GEO) under accession numbers GSE142321 and GSE142322.

[1]F. Roudnicky and J.D.Z. contributed equally to this work.

[2]To whom correspondence may be addressed. Email: jitao_david.zhang@roche.com, peter.westenskow@roche.com, or chadacowan@gmail.com.

[3]C.A.M., P.D.W., and C.A.C. contributed equally to this work.

This article contains supporting information online at https://www.pnas.org/lookup/suppl/doi:10.1073/pnas.1911532117/-/DCSupplemental.

First published August 5, 2020.

Significance

Blood vessels in the central nervous system possess unique barrier properties that prevent infiltration of foreign substances and allow for precise delivery of ions, molecules, and immune cells into neural networks. Barrier breakdown is associated with a host of retinal and neurological disorders but few BRB/BBB-enhancing therapies have been developed. To identify novel barrier-inducing factors, we genetically engineered a transcriptional reporter cell line with CRISPR technology for compound library screening. Using this approach, we identified compounds, including a TGF-β receptor inhibitor, RepSox, which functions in vitro to increase barrier resistance in human primary and stem cell-derived endothelial cell lines. These data may inform future therapies for BRB/BBB disorders and retinal/neurological diseases.

To create an optimized CNS-EC model, we generated a reporter cell line with a surrogate fluorescent marker of vascular permeability, performed flow cytometry-based chemogenomic library screening on those cells, and tested one candidate compound in vitro and in vivo. GFP was inserted in frame with CLDN5 using genome-editing technology in human pluripotent stem cell (hPSC)-ECs (13). The hPSCs harboring CLDN5-GFP were then differentiated to endothelial cell fates (hPSC-ECs) (14, 15) using a simple and scalable protocol we developed (16, 17). We then subjected CLDN5-GFP hPSC-ECs to compounds in Small-molecule PAthway Research Kit (SPARK), a chemogenomic library that we constructed, and observed that several compounds, including RepSox and other TGF-β receptor inhibitors, increased GFP fluorescence in CLDN5-GFP hPSC-ECs. When tested in orthogonal assays, RepSox induced EC barrier stability in cultured ECs, regulated a host of key BRB/BBB characteristic factors, and influenced vascular patterning in vivo. The findings suggest that the compound may be used for generating BRB/BBB models and for finding novel therapies for patients with deterioration of functions or pathological changes of BRB/BBB.

Results

Claudin-5 was selected as the junctional protein reporter gene for this study based on published gene-profiling data from isolated BBB-ECs (7, 8) and our own observations. CLDN5 is one of the highest expressed genes (7, 8) and the most highly expressed tight junction gene in BBB-ECs (Fig. 1*A*). The CLDN5-P2A-GFP fusion reporter EC line was generated using the CRISPR/Cas9 gene editing strategy depicted in *SI Appendix*, Fig. S1*A*. Briefly, the targeting vector was engineered to contain sequences from the 3′ end of CLDN5 tagged with a P2A self-cleaving peptide, a promoter-less P2A-GFP sequence flanked by two homology arms (HAs), and a resistance cassette flanked by PiggyBac transposase inverted terminal repeats (ITRs) to allow traceless excision (*SI Appendix*, Fig. S1*B* and Dataset S1). Cas9 and a specific single guide RNA-containing sequence near the stop codon of CLDN5 catalyzed a double-stranded break in the target genomic sequence, which was then repaired through homologous recombination between CLDN5 and the donor template (*SI Appendix*, Fig. S1*C*). Then, the resistance cassette was removed using an excision-only PiggyBac transposase (*SI Appendix*, Fig. S1*D*). To confirm that gene replacement occurred correctly, qPCR was used to detect the loss of the vector tTK sequence (*SI Appendix*, Fig. S1*E*, black bars, "negative" clones). These clones were then evaluated by PCR for correct insertion of GFP (*SI Appendix*, Fig. S1 *F*, *Left*) and lack of tTK (*SI Appendix*, Fig. S1 *F*, *Right*) using primers provided in *SI Appendix*, Fig. S1 *C* and *D*. Three clones with correct insertions were further confirmed by Sanger sequencing (*SI Appendix*, Fig. S1*G*). The other two were normal and had normal karyotype G-banding patterns (*SI Appendix*, Fig. S1*H*).

Using our previously published protocol (16, 17), we differentiated both wild-type (WT) and CLDN5-GFP hPSC lines into EC fates and observed that 15 to 25% (Fig. 1*B*, depending on the clone) of the cells from the reporter line were GFP-positive (CLDN5-GFP$^+$) and, as expected, none of the WT cells expressed GFP. CLDN5-GFP hPSC-ECs were then sorted by fluorescence-activated cell sorter (FACS) into CLDN5-GFP$^+$ and CLDN5-GFP$^-$ populations and studied independently. First, we measured barrier resistance using electric cell-substrate impedance sensing (ECIS) and detected a 1.75-fold increase in resistance in CLDN5-GFP$^+$ hPSC-ECs (Fig. 1*C*) versus CLDN5-GFP$^-$ hPSC-ECs.

Next, we profiled both messenger RNA (mRNA) and protein expression using RNA-seq (Dataset S2) and target mass tags (TMT)-MS3 mass spectrometry protein expression profiling (Dataset S4), respectively. Both CLDN5-GFP$^+$ and CLDN5-GFP$^-$ hPSC-ECs displayed endothelial cell markers (high VE-Cadherin [endothelial marker, CDH5], and no E-Cadherin [epithelial marker, CDH1] expression) (*SI Appendix*, Fig. S2*A*). Next, we generated the *BioQC* (18) enrichment score (Dataset S3) of all primary cell expression signatures from the FANTOM 5 database (19) by using expression profiles of individual samples of CLDN5-GFP$^+$ or CLDN5-GFP$^-$ cells (*SI Appendix*, Fig. S2 *B* and *C*). Since the enrichment score varies strongly by cell type but barely by samples, we aggregated them by cell-identity signatures and derived average enrichment scores across samples (*SI Appendix*, Fig. S2 *B* and *C*). Among all primary cell signatures derived from FANTOM 5, we found that the enrichment of signature genes of ECs is much stronger than enrichment of signature genes of non-ECs, and this applies to many different types of ECs (*SI Appendix*, Fig. S2*B*). When we examined signatures that reported *BioQC* enrichment score equal or larger than 5 (unadjusted $P <$ 1E−5, one-sided Wilcoxon-Mann–Whitney U test) in at least one sample, we found that out of the ten signatures that met this filtering criteria, nine are endothelial-cell signatures (*SI Appendix*, Fig. S2*C*), which exhaust EC-identities indexed by the FANTOM 5 database. The results suggest that hPSC-derived ECs resemble more closely primary ECs than any other cell types indexed by the FANTOM 5 database.

We observed that in CLDN5-GFP$^+$ and CLDN5-GFP$^-$ hPSC-ECs transcriptomic and proteomic expression profiles are substantially correlated (Spearman correlation $r = 0.79$, $P < 0.0001$) (Fig. 1*D*). We confirmed that CLDN5 transcripts and proteins were up-regulated in GFP-positive cells (Fig. 1*E*) and detected increases in expression of tight junction components OCLN (Fig. 1*F*) MARVELD2, and MARVELD3, although the reads per kilobase of transcript, per million mapped reads (RPKM) values were low (on RNA level only) (Fig. 1*G* and Dataset S15) while TJP1 expression was unchanged (Fig. 1*F*). Similar effects were detected in adhesion receptor PECAM1 and CDH5 expression (Fig. 1*F*). Transcripts for the gap junctions *GJA3*, *GJA4*, and *GJA5* (*SI Appendix*, Fig. S2*D*) were up-regulated, and *CGN*, *ESAM*, and *JAM3* were unchanged (*SI Appendix*, Fig. S2*E*). *ABCA1*, *ABCC4*, and *SCARB1* transporter genes were up-regulated, but no change in protein production was detectable (Fig. 1*H*). Several other transporter genes that showed up-regulated mRNA level, including *ABCA2*, *ABCB1*, *ABCG1*, and *SLC6A8*, were not detected by TMT-MS3 mass spectrometry protein expression profiling (Fig. 1*I*). There was no significant difference in mRNA or protein expression of ABCC1 and ABCA3 (*SI Appendix*, Fig. S2*F*), and *INSR* mRNA transcripts were up-regulated, but no changes in *LRP1* were observed, and *MFSD2A* was down-regulated (*SI Appendix*, Fig. S2*G*). Glucose transporter SLC2A1 (GLUT1) was down-regulated (Fig. 1*J*), and no significant differences were observed in KDR or CD34 expression (Fig. 1*K*). Cumulatively, the results may suggest that increased CLDN5 expression correlates with stronger barrier properties in ECs.

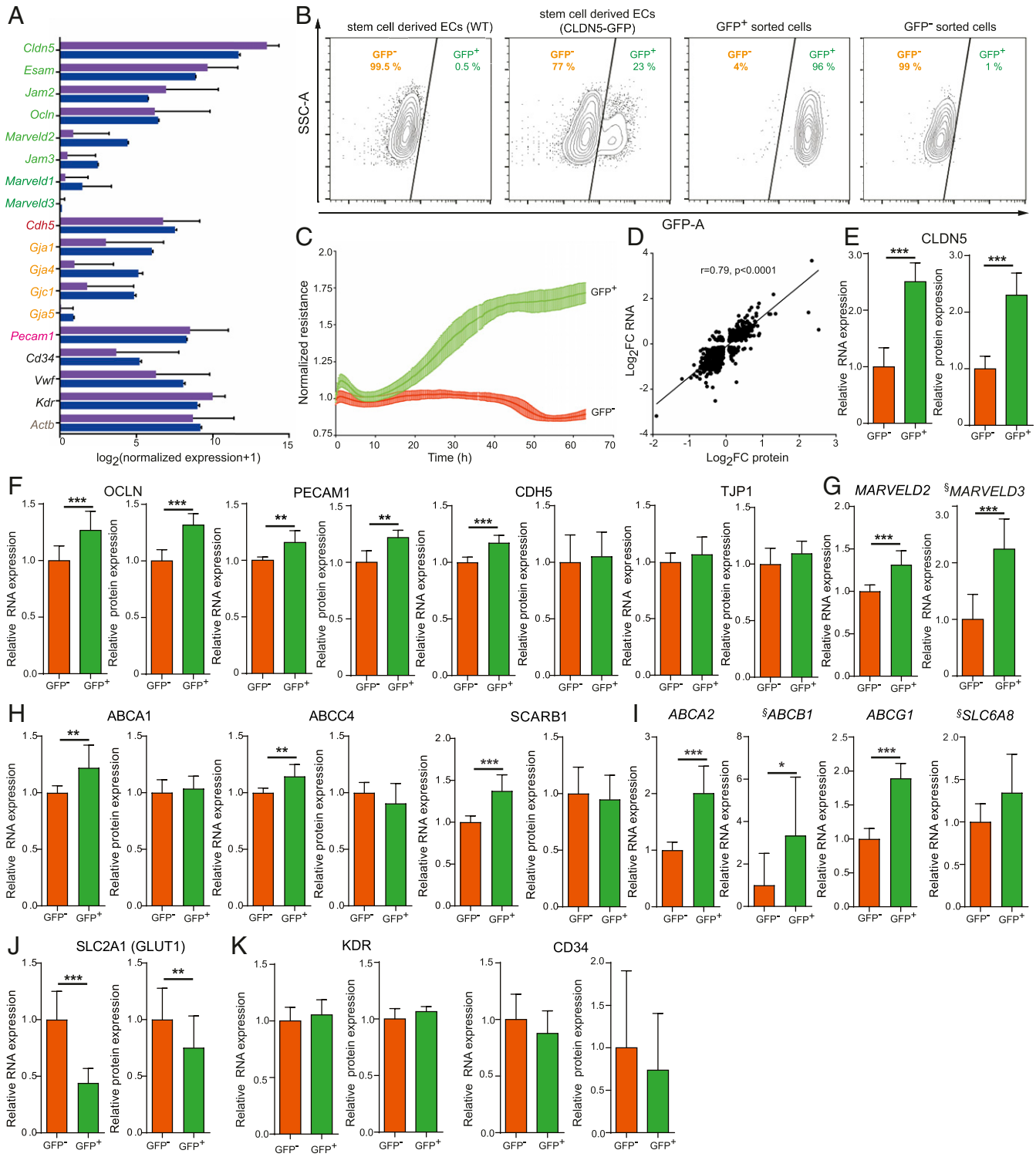

Fig. 1. Characterization of hPSC-derived endothelial cells carrying a CLDN5-tagged GFP reporter. (*A*) RNA-seq of ex vivo isolated ECs from the BBB with normalized expression for proteins involved in EC junction formation indicated as follows: purple bars represent data from Vanlandewijck et al. (8); blue bars represent data from Zhang et al. (7). For gene names, the color indicates the cellular function: tight junctions (green), adherens junctions (red), gap junctions (orange), adhesion molecule (pink), endothelial cell markers (black), and housekeeping gene (gray). Mean normalized $\log_2$ expression was plotted with ±SD. (*B*) FACS analysis of hPSC-derived ECs, either WT or CLDN5-GFP hPSC-ECs (one clone), sorted by FACS into CLDN5-GFP$^+$ or CLDN5-GFP$^-$ population (*Left Two Panels*). The *Right Two Panels* represent FACS analysis of CLDN5-GFP reporter cells separated into either the CLDN5-GFP$^+$ population or the CLDN5-GFP$^-$ population. (*C*) ECIS of CLDN5-GFP hPSC-ECs sorted into CLDN5-GFP$^+$ and CLDN5-GFP$^-$ populations measured in real time. (*D*) Spearman correlation of significantly up- or down-regulated proteins and their respective mRNAs as measured by mass spectrometry and RNA-seq. (*E*–*G*) CLDN5-GFP hPSC-ECs sorted into CLDN5-GFP$^+$ and CLDN5-GFP$^-$ populations were analyzed for relative overall mRNA and protein expression: (*E*) CLDN5 and (*F*) RNA-seq and mass spectrometry data of tight junction-related proteins including OCLN, PECAM1, CDH5, and TJP1. (*G*) RNA-seq data for MARVELD2 and MARVELD3. (*H*) RNA-seq and mass spectrometry data of transporter-related proteins including ABCA1, ABCC4, and SCARB1 and (*I*) *ABCA2*, *ABCB1*, *ABCG1*, and *SLC6A8*. (*J*) RNA-seq and mass spectrometry data for SLC2A1 (GLUT1). (*K*) KDR and CD34 expression. §, The low RPKM average values for MARVELD3, ABCB1, and SLC6A8 (average RPKM < 1) (Dataset S15). Columns show means ± SD. *FDR <0.05, **FDR <0.01, ***FDR <0.001.

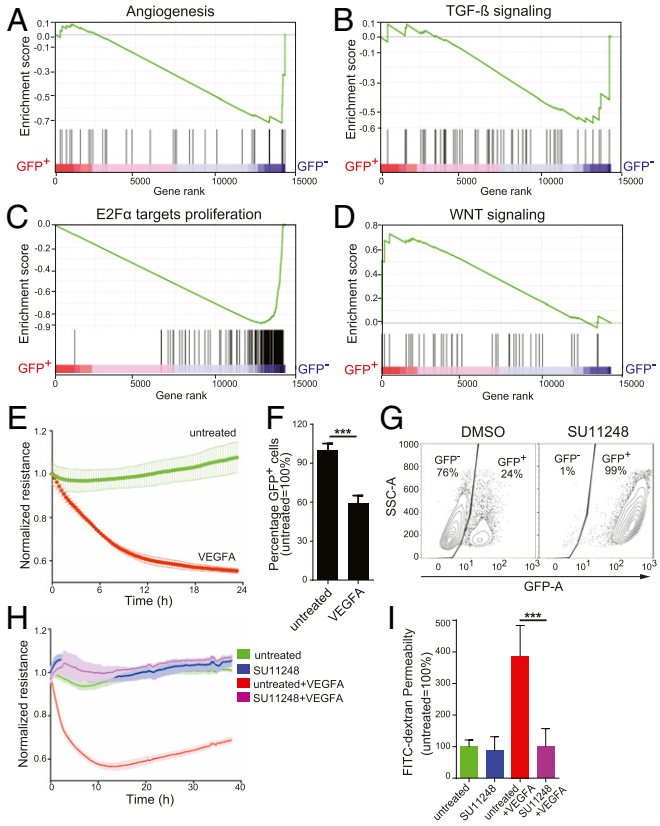

Fig. 2. The GFP$^+$ population of CLDN5-GFP reporter ECs has both the gene expression signature and functional response of endothelial cell barriers. (*A*–*D*) Gene set enrichment analysis (GSEA) enrichment plots of CLDN5-GFP$^+$ or CLDN5-GFP$^-$ populations of CLDN5-GFP hPSC-ECs for pathways relevant to barrier functions: (*A*) angiogenesis, (*B*) TGF-β, (*C*) E2Fα proliferation, and (*D*) Wnt signaling. The enrichment scores (ESs) are plotted at the top of each panel, and a value of the ranking metric throughout the list of ranked genes is depicted at the bottom of each panel (from left to right). Genes were ranked by the product of $\log_2$-FC and negative log of FDR value. (*E*) The CLDN5-GFP$^+$ hPSC-EC population was stimulated with 50 ng/mL VEGFA, and ECIS was measured in real time. (*F*) After 48 h of VEGFA treatment, the relative percent of CLDN5-GFP$^+$ hPSC-ECs was measured using FACS. (*G*–*I*) CLDN5-GFP hPSC-ECs were treated with the tyrosine kinase inhibitor SU11248 (at 5 μM for 48 h) or with a DMSO control and analyzed as follows: (*G*) The percentage of CLDN5-GFP$^+$ hPSC-ECs was quantified using FACS, *y* axis represents side-scatter area; (*H*) impedance was measured in real time; and (*I*) FITC-dextran permeability was measured. Columns are means ± SD. The permeability assays and impedance measurements were performed as three independent experiments with at least three replicates. ***$P < 0.001$.

To explore pathway-level differences between CLDN5-GFP$^+$ and CLDN5-GFP$^-$ hPSC-ECs, we performed gene-set enrichment analysis on gene expression data using the hallmark gene set in the Molecular Signatures Database (MsigDB) (20). $\log_2$-fold change (FC) and the –log10 false discovery rate (FDR) of selective pathway modulation are summarized in Datasets S5*A* and S5*B*. The results suggested that in CLDN5-GFP$^+$ hPSC-ECs the following pathways are inhibited: angiogenesis (Fig. 2*A* and *SI Appendix*, Fig. S3*A*), TGF-β (Fig. 2*B* and *SI Appendix*, Fig. S3*B*), and E2Fα-proliferation (Fig. 2*C* and *SI Appendix*, Fig. S3*C*). However, Wnt signaling genes (Fig. 2*D* and *SI Appendix*, Fig. S3*D*) are activated in CLDN5-GFP$^+$ hPSC-ECs.

To test the permeability properties, CLDN5-GFP hPSC-ECs were challenged with vascular endothelial growth factor A (VEGFA) (21, 22), a potent vascular permeability-inducing factor, and we measured their barrier properties. The addition of VEGFA induced a rapid drop in measured resistance values (Fig. 2*E*) and decreased the population of CLDN5-GFP$^+$ (Fig. 2*F*). Conversely, inhibiting tyrosine kinase receptors with SU11248 (Sunitinib) (23) resulted in a striking increase in the proportion of CLDN5-GFP$^+$ hPSC-ECs (99%) (Fig. 2*G*), and SU11248-treated cells were less sensitive to VEGFA-induced permeability in ECIS (Fig. 2*H*) and fluorescein isothiocyanate (FITC)-dextran permeability assays (Fig. 2*I*). This observation supports the notion that CLDN5-GFP could be a faithful surrogate of EC barrier status.

We next set out to screen CLDN5-GFP hPSC-ECs to identify novel barrier-inducing agents. As a first step, we generated a small-molecule compound library that contains small molecules with high potency and selectivity for human druggable genes annotated to cellular pathways, which we named Small-molecule PAthway Research Kit (SPARK). We achieved this by integrating quantitative activity information derived from dose–response data from both proprietary information of F. Hoffmann-La Roche Ltd and the publicly available ChEMBL database (24). We constructed the Compound-Activity-Target (CAT) database in which the targets are indexed by UniProt IDs (25) and Entrez GeneIDs (26) and small molecules are indexed by InChIKeys, a hashed version of full International Chemical Identifiers (InChI) (Fig. 3*A*). The activity is represented by *pAct*, the absolute values of common logarithm transformed affinity measurements (dissociation constant [K_d], inhibition constant [K_i], concentration that inhibits response by 50% [IC_{50}], or effective concentration, 50% [EC_{50}]). In case multiple bioactivity measurements were available for a compound-target pair, the measurements were averaged. In order to identify a set of representative compounds that target the druggable genome, we applied an unsupervised learning approach by clustering compounds based on their target profiles using the Affinity Propagation clustering method (27), resulting in 1,158 compound clusters. In parallel, the Gini Index was employed to characterize the specificity of the compounds using *pAct* values for individual target genes (18, 28). A Gini Index near 1.0 indicates that the compound is highly specific for one target (or target gene family) while a Gini Index near 0.0 indicates the compound is promiscuous (Fig. 3*B*). We selected representative compounds with either the highest Gini Index (i.e., most specific) (Fig. 3*B*) or the highest *pAct* value (i.e., most potent) (Fig. 3*C*) with regard to the genes targeted by the compounds in each cluster; when the two criteria recommend two compounds, both are taken. Lastly, we manually curated the compounds, removed those that were not suitable for high throughput screening (HTS) assays or were unavailable, and replaced with similar compounds whenever possible. The outcome was a library of 2,059 unique small molecules (Dataset S6), targeting in total 1,466 unique human genes (Dataset S7) with activity of 1 μM or lower. We compared the SPARK library with the CAT database and confirmed that SPARK compounds have significantly higher specificity (median Gini Index around 0.6) than those in CAT (median Gini Index less than 0.1) (Fig. 3*B*) and are on average ∼100 times more potent (median *pAct* ∼8, or activity ∼10 nM versus median *pAct* ∼6, or activity ∼1 μM) (Fig. 3*C*). Finally, we compared the distribution of several molecular descriptors of the compounds in both databases (Fig. 3*D*) and found no significant differences ($P > 0.05$, Wilcoxon test for continuous variables and $\chi 2$ test for discrete variables), suggesting that SPARK uniformly samples the chemical space spanned by the CAT database.

To annotate the library in terms of biological pathways, 1,446 target proteins were mapped to 193 distinct UniProt keywords that fall into 24 target classes (Fig. 3*E* and Dataset S8). In parallel, the proteins were mapped to 905 gene sets defined by the Reactome database (29), the Kyoto Encyclopedia of Genes and Genomes (KEGG) database (30), and Gene Ontology (GO) Biological Process (BP) terms (31), which form 142 human pathway clusters (Dataset S9 and *SI Appendix*, Fig. S4) by unsupervised clustering. The pathway clusters in turn were manually mapped into 16 top-level pathway categories as defined by

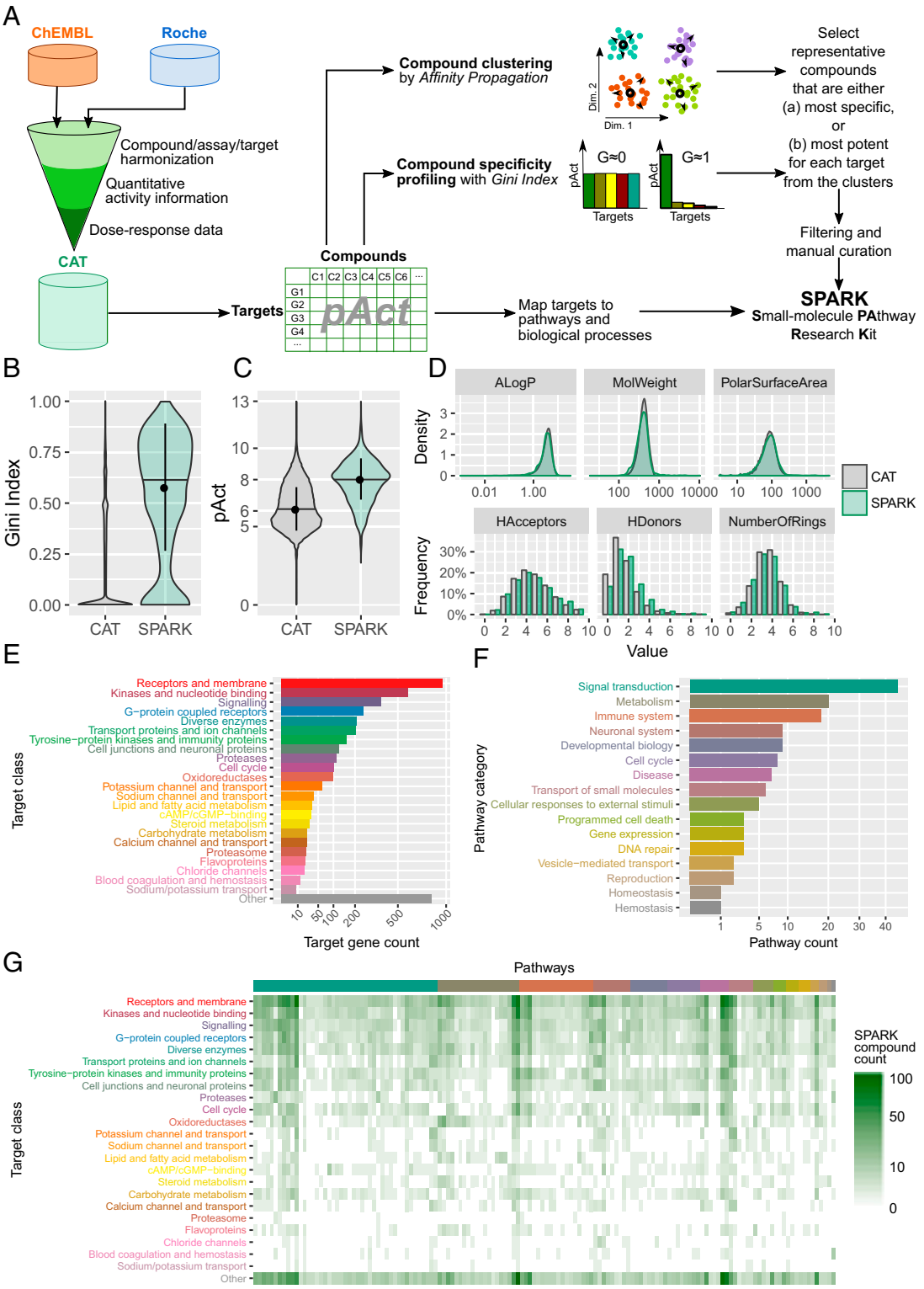

Fig. 3. Design and characterization of SPARK, a chemogenomic library. (*A*) A schematic of the workflow used to establish the CAT database and construct the SPARK library. (*B–D*) A comparison of the compounds in the CAT database and in the SPARK library in terms of (*B*) Gini Index values, (*C*) *pAct* values against primary targets, and (*D*) profiles of molecular descriptors, which include: ALogP, an estimate of the molecular hydrophobicity (lipophilicity) defined as the logarithm of the 1-octanol/water partition coefficient; MolWeight, molecular weight (in daltons); PolarSurfaceArea, defined as the surface sum over all polar atoms; HAcceptors, proton acceptors; HDonors, proton donors; NumberOfRings, number of aromatic rings. (*E*) Protein classes targeted by compounds in the SPARK library (filtered by median of *pAct* ≥ 6) as defined by UniProt keywords. Bars show the count of unique target genes in each class. (*F*) Biological pathway categories associated with target genes of SPARK compounds, defined by a combination of Reactome pathways, KEGG pathways, and GO BP terms, and consolidated by a heuristic fuzzy partition algorithm. Bars show the count of unique pathways in each category. (*G*) A heat map of SPARK compounds that target proteins of a given class (in rows) and within a given biological pathways (in columns). Target classes follow the same order as in *E*. Pathways are organized by categories in the same order as in *F*. Within each category, pathways are ordered by hierarchical clustering.

the Reactome database (Fig. 3*F*). In summary, SPARK library compounds are characterized by both target class and biological pathways (Fig. 3*G*).

We screened the SPARK library on CLDN5-GFP hPSC-ECs and used FACS to detect changes in CLDN5-GFP$^+$ expression 48 h posttreatment (Fig. 4*A*). Sixty-two compounds induced at least twofold increase compared to dimethyl sulfoxide (DMSO) controls (>31.7% CLDN5-GFP$^+$) (Fig. 4*A* and Dataset S10). We could map most of them to a few target classes defined by UniProt keywords, including enzymes, membrane receptors, transcription factors, and ion channels (Fig. 4*B* and Dataset S10). We further performed dose–response experiments (*SI Appendix*, Fig. S5 *A–F*), measured barrier-promoting activity using ECIS, and performed FITC-dextran permeability assays for six of the most potent compounds (Fig. 4 *C–H*). One of these compounds, LY215729 (a TGF-β pathway inhibitor), promoted barrier activity in resting ECs and partially prevented the disruptive effects of VEGFA. This is consistent with our observation that the TGF-β pathway was down-regulated in CLDN5-GFP$^+$ hPSC-ECs (Fig. 2*B*).

Using functional barrier assays, we compared the effects of TGF-β–inhibiting compounds in VEGFA untreated and treated cells (Fig. 5 *A*, *Left* and *Right*). Of the five tested, RepSox induced the strongest effect on EC barrier properties (Fig. 5*A*). To determine TGF-β pathway specificity, we tested four annotated TGF-β pathway inhibitory compounds: RepSox, GW788388, and SB505124 that all enhanced EC barrier resistance and integrity, and SB431542 that was inactive in barrier assays. As expected, all four compounds inhibited the TGF-β pathway kinases ACVR1B (ALK4) and TGFBR1 (ALK5), but only the two most potent compounds (RepSox and GW788388) inhibited TGFBR2 (strongly) and BMPR1B (weakly) (*SI Appendix*, Fig. S6*A*). Each of the four compounds had K_d values for ACVR1B (ALK4) and TGFBR1 (ALK5) in the nanomolar range. RepSox and GW788388 were the most potent inhibitors of ACVR1B (ALK4), TGFBR1 (ALK5), and TGFBR2, and also had K_d values in the nanomolar range for ACVR2B (ALK4), BMPR1B, and JNK2 (*SI Appendix*, Fig. S6*B*).

We went on testing the barrier-modulating potential of RepSox using transendothelial electrical resistance (TEER) assays without or with VEGFA (Fig. 5 *B* and *C*) in different endothelial cell types, including hPSC-ECs, human brain microvascular endothelial cells (hBMECs), and human retinal microvascular endothelial cells (hRMECs). As observed in ECIS and TEER assays, RepSox significantly reduced endothelial permeability in FITC-dextran permeability assays (4 and 40 kDa) in hPSC-ECs (Fig. 5*D*), in

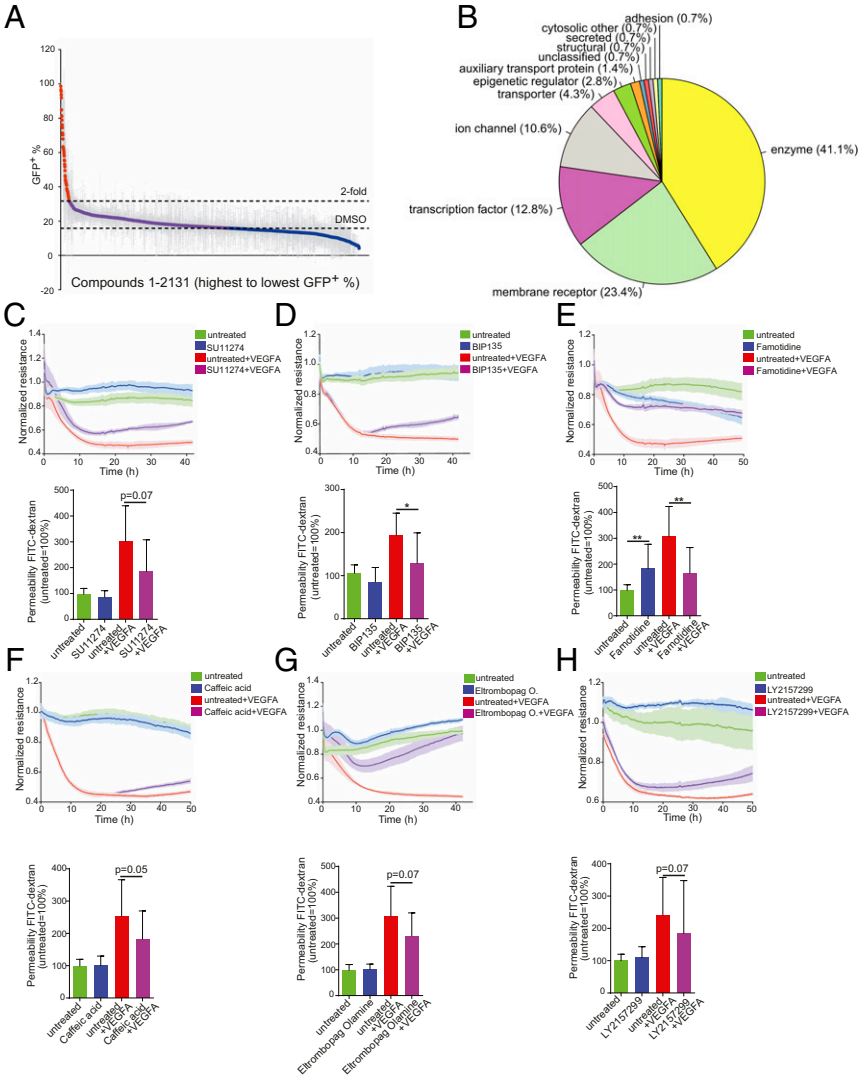

Fig. 4. Identification of compounds from the SPARK library that induce endothelial cell barrier resistance. (*A*) Compounds from the SPARK library, used at 5 μM, were tested in duplicate, and the percent of CLDN5-GFP$^+$ hPSC-ECs was evaluated 48 h posttreatment. Each dot represents a distinct compound, and those plotted in red induced greater than twofold mean induction of CLDN5-GFP$^+$ hPSC-ECs over the DMSO control. (*B*) The 62 compounds that induced a greater than twofold induction of CLDN5-GFP$^+$ hPSC-ECs mapped to several target classes, as indicated. (*C–H*) Functional evaluation (*Upper*, ECIS analysis; *Lower*, FITC-dextran permeability assay) of representative compounds from differing target classes: (*C*) SU11274, (*D*) BIP135, (*E*) Famotidine, (*F*) Caffeic acid, (*G*) Eltrombopag olamine, (*H*) LY2157299. Columns are means ± SD. The permeability assays and impedance measurements were performed as three independent experiments with at least three replicates. $^{**}P < 0.01$, $^{*}P < 0.05$.

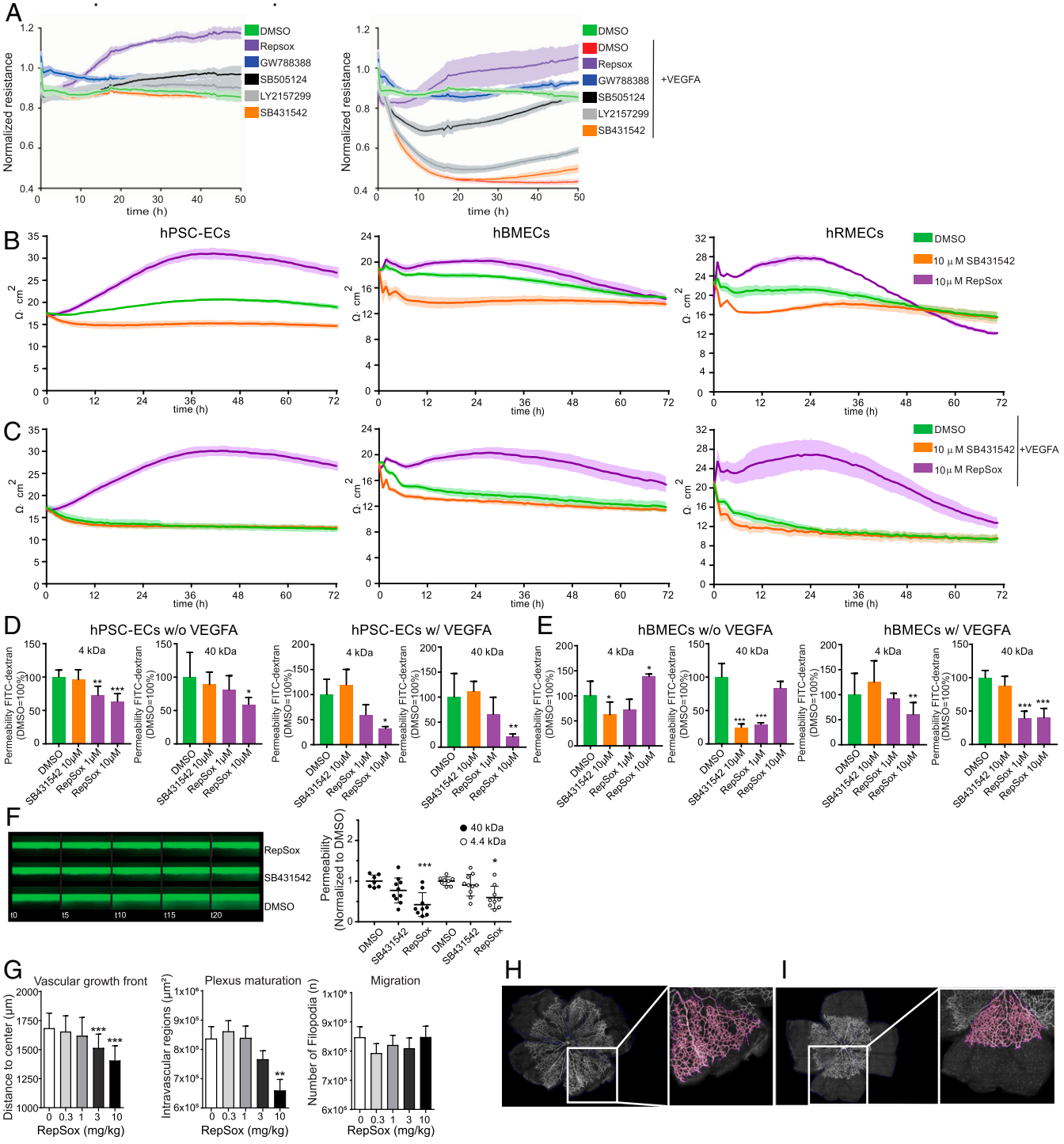

Fig. 5. Functional barrier evaluation after treatment with RepSox and SB431542. (*A*) CLDN5-GFP hPSC-ECs were analyzed by ECIS in the presence and absence of five different TGF-β pathway inhibitors without (*Left Graph*) or with (*Right Graph*) the addition of VEGFA. Compounds are shown based on capability to induce barrier, top to bottom. (*B*) The absolute TEER values (Ω·cm^2) after treatment with DMSO or 10 μM SB431542 or 10 μM RepSox on (*Left*) hPSC-ECs, (*Middle*) hBMECs, and (*Right*) hRMECs. (*C*) The absolute TEER (Ω·cm^2) values with cotreatment of VEGFA and compounds, DMSO, 10 μM SB431542, or 10 μM RepSox on (*Left*) hPSC-ECs, (*Middle*) hBMECs, and (*Right*) hRMECs. All TEER assays were performed as at least three independent experiments with three replicates for each condition. (*D* and *E*) The FITC-dextran (4 and 40 kDa) permeability assay. (*D*, *Left*) hPSC-ECs treated with DMSO, 10 μM SB431542, or 10 μM RepSox and (*D*, *Right*) cotreated with VEGFA and DMSO, 10 μM SB431542, or 1 and 10 μM RepSox. (*E*, *Left*) hBMECs treated with DMSO, 10 μM SB431542, or 1 and 10 μM RepSox and (*E*, *Right*) cotreated with VEGFA and DMSO, 10 μM SB431542, or 1 and 10 μM RepSox. (*F*) The barrier on-a-chip assay with hRMECs. (*Left*) Barrier integrity assay in hRMEC: 40-kDa FITC-dextran solution is perfused in the endothelial tube, and leakage in the adjacent channel is monitored over the course of 20 min. (*Right*) apparent permeability of hRMEC to 40 kDa and 4.4 kDa dextran. Results represent means ± SD and were normalized to DMSO control. (*G*) Segmentation and quantification of vascular sprouting in a flat mounted newborn mouse retina after treatment with RepSox in a dose–response. (*Left*) The radial expansion of the vascular front was measured as distance from the center to the peripheral retinal. (*Middle*) Plexus maturation was calculated as the mean area of intravascular lesions representing the primitive plexus area. (*Right*) Migration was estimated based on the number of filopodia. (*H* and *I*) Representative images of segmented retinal flat mounts (pink) computationally traced vessels in the retina: (*H*) control treated and (*I*) treated with 3 mg/kg RepSox, respectively with magnification at 20×. Columns are means ± SD. *$P < 0.05$, **$P < 0.01$, ***$P < 0.001$.

hBMECs (Fig. 5*E*), and in the hRMECs three-dimensional barrier model (Fig. 5*F*).

Furthermore, exogenous RepSox delivery in neonatal mice resulted in dose-dependent vascular patterning defects (Fig. 5 *G–I*). In these neonatal mice treated with RepSox, measurements of the radial distance from the optic nerve in retinal flat mounts revealed that RepSox significantly and dose-dependently reduced propagation of the angiogenic front (Fig. 5 *G* and *I*; labeled "Vascular growth front") compared to controls (Fig. 5 *G* and *H*). Closer analyses revel that the empty area between capillaries was also reduced (Fig. 5*G*; labeled "Plexus maturation"), but the number of tip-cell microvilli was unchanged in RepSox treated pups (Fig. 5*G*; labeled "Migration"). However, RepSox did not rescue the excessive permeability observed in an acute disease model, laser-induced choroidal neovascularization (CNV) rats (*SI Appendix*, Fig. S7).

To elucidate the barrier-promoting molecular mechanisms of RepSox, we performed transcriptomic profiling with RNA-seq at two different time points (8 and 48 h) after treatment of ECs with either DMSO, SB431542, or RepSox (Fig. 6 *A–G* and Dataset S11). Using the hallmark gene set at the MsigDB, we performed gene-set enrichment analysis on cells treated with either the most active compound, RepSox (*SI Appendix*, Fig. S6*C* and Datasets S12*A*–S12*D*), or the least active compound, SB431542 (*SI Appendix*, Fig. S6*D* and Datasets S12*A*–S12*D*), and sorted genes by the product of log-FC and negative log-10 transformation of the *P* values. As expected, TGF-β pathway inhibition was observed for both compounds, but other pathways were differentially regulated (*SI Appendix*, Fig. S6 *C* and *D*, marked in green; and Datasets S12*A*–S12*D*). Notably, RepSox acts in an opposite manner of VEGFA, a proangiogenic and permeability-inducing factor, by strongly up-regulating the tight junction protein-related gene *CLDN5* and down-regulating *PLVAP*, a protein associated with highly permeable blood vessels (Fig. 6*A* and *SI Appendix*, Fig. S6*E*) (32, 33). Neither SB431542 nor RepSox delivery affected expression of *KDR* or *PECAM1* genes after 8 h although a slight down-regulation of *PECAM1* and *KDR* was observed after 48 h (Fig. 6*B*). Next, we measured expression of genes involved in angiogenesis (EC sprouting) and observed that RepSox inhibited the sprouting-promoting gene *ESM1* (34) (Fig. 6*C* and *SI Appendix*, Fig. S6*F*) and up-regulated sprouting inhibitory genes *HEY1*, *HEY2*, and *FLT1* (Fig. 6*C* and *SI Appendix*, Fig. S6*B*). The effect on ESM1 is consistent with the antiangiogenic activity of RepSox as in the in vivo sprouting assay (Fig. 5 *G–I*) and measured by kinase assay (*SI Appendix*, Fig. S6*B*). RepSox also inhibited expression of inflammation-related genes *NFATC2*, *JAK1*, *JAK3*, and *ICAM1* (Fig. 6*D*). Furthermore, RepSox potently activated Wnt-signaling genes *AXIN2*, *TNFRSF19*, *APCDD1*, *FZD4*, and *LRP6* (*GSK3β* was down-regulated) (Fig. 6*E*). Both SB431542 and RepSox significantly down-regulated TGF-β pathway members *ALK5* (*SERPINE1*, *PDGFB*, *TGFBI*, and *CTGF*) (Fig. 6*F*), but only RepSox inhibited *ALK1* (*ID1* and *LRG1*) (Fig. 6*G*). Proteomic analyses revealed that RepSox down-regulated inflammatory response-related proteins (FLT1, ICAM1, and KDR) (Fig. 6*H* and Datasets S13 and S14) while increased expression of tight junctional proteins CGN and SHROOM1, and gap junction proteins GJA4 and GJA5. (Fig. 6*I* and Datasets S13 and S14). In addition, we observed that transporter proteins ABCC1, SLC2A1, SLC3A2, and TFRC were up-regulated (Fig. 6*J* and Datasets S13 and S14).

To validate the findings of mRNA and protein expression modulation, we also examined the effects of RepSox treatment using immunocytochemistry. The level of fluorescence intensity of VE-Cadherin was not significantly changed by DMSO, SB431542, and RepSox treatment without VEGF or with VEGF in hPSC-ECs and hBMECs (*SI Appendix*, Fig. S8). Therefore, the area of VE-Cadherin staining was chosen as the area of interest for further quantification. Expression of Claudin-5, ZO-1, and Occludin overlapped with VE-Cadherin and was enriched in cell membranes (Figs. 7 and 8). ZO-1 was highly expressed in RepSox-treated hPSC-ECs (Fig. 7 *A* and *C*), and Claudin-5 was up-regulated in hBMECs with RepSox treatment (Fig. 7 *B* and *C*). Semiquantitative methods revealed VEGFA/RepSox cotreatments induced Occludin in hPSC-ECs (Fig. 8 *A* and *C*). Claudin-5, ZO-1, and Occludin were all up-regulated in hBMECs, up to sixfold, 1.5-fold, and 3.2-fold, respectively (Fig. 8 *B* and *C*). To explore the effect of RepSox on transcytosis, we treated cells with cholera toxin subunit B (CtxB) and counted the number of conglomerates taken up into the cytosol. The number of conglomerates of CtxB was suppressed in the RepSox-treated hPSC-ECs compared to the DMSO control. The translocation reduction of CtxB with RepSox treatment occurs in a caveolae-independent way as there were no substantial changes of the Caveolin-1 fluorescent signal in confocal images (*SI Appendix*, Fig. S9).

Discussion

Here, we report an innovative approach of generating a monolayer model of CNS-ECs. We introduced a workflow that combines genome editing, stem cell differentiation to ECs, and compound profiling to identify compounds and pathways that modulate CLDN5 expression and EC barrier integrity. CRISPR/Cas9 technology was used to generate a CLDN5-P2A-GFP fusion reporter in an hPSC cell line, and differentiation to ECs revealed a subpopulation of ECs that were CLDN5-GFP–positive. This is not surprising as stem cell differentiation protocols generate a mixed subpopulation of differentiated cells (35, 36). CLDN5-GFP$^+$ hPSC-ECs displayed higher barrier resistance values than CLDN5-GFP$^-$ hPSC-ECs. Importantly, we observed that the CLDN5-GFP$^+$ hPSC-ECs featured higher expression of several tight junctions and transporters characteristic of CNS-ECs on both RNA and protein levels. Our data confirmed previous findings that CLDN5 is dynamically regulated to modulate resistance between ECs and suggest that its expression would be a faithful reporter of vascular barrier stability. This is in agreement with preclinical studies that have shown that Claudin-5 is the most enriched tight junction in CNS-ECs and it is important for barrier establishment and maintenance (37, 38), and that dosage of Claudin-5 is critical for neuronal functions (10, 11).

In order to find cellular pathways that modulate CLDN5 and EC barrier resistance, we constructed SPARK, an unbiased library of specific and potent small molecules that are annotated with both molecular targets and likely relevant biological pathways. So far, most compound libraries have been constructed through manual selection (39) (e.g., LOPAC, Prestwick), but recently there have been efforts to generate chemogenomic libraries using: 1) repurposed clinically tested candidates (40), 2) peer review catalogs (41), or 3) objective computer-assisted prioritization of chemical probes for specificity and potency (42–44). SPARK was generated by mining of both publicly available and proprietary data and manual curation to annotate the compounds with associated biological pathways and targets. Using our reporter CLDN5-P2A-GFP hPSC-ECs, we screened the SPARK library and identified pathways that regulate EC barrier, including the Wnt, VEGFA, and TGF-β pathways.

Sorted CLDN5-GFP$^-$ hPSC-ECs subpopulation showed an increased expression of TGF-β pathway molecules compared to CLDN5-GFP$^+$ hPSC-ECs, and previous studies suggested that the TGF-β pathways play a role in barrier formation as SB431542 (a TGFBR1 [ALK5] inhibitor) induces CLDN5 expression (45) and CDH5 (VE-Cadherin), a major adhesion factor, interacts with the TGF-β R1/R2 complex (46, 47). Therefore, we performed a focused screen of publicly available TGF-β pathway inhibitors and identified RepSox as the strongest inducer of EC barrier resistance as measured by ECIS, TEER, and FITC-dextran permeability assays (4 and 40 kDa). TEER values were

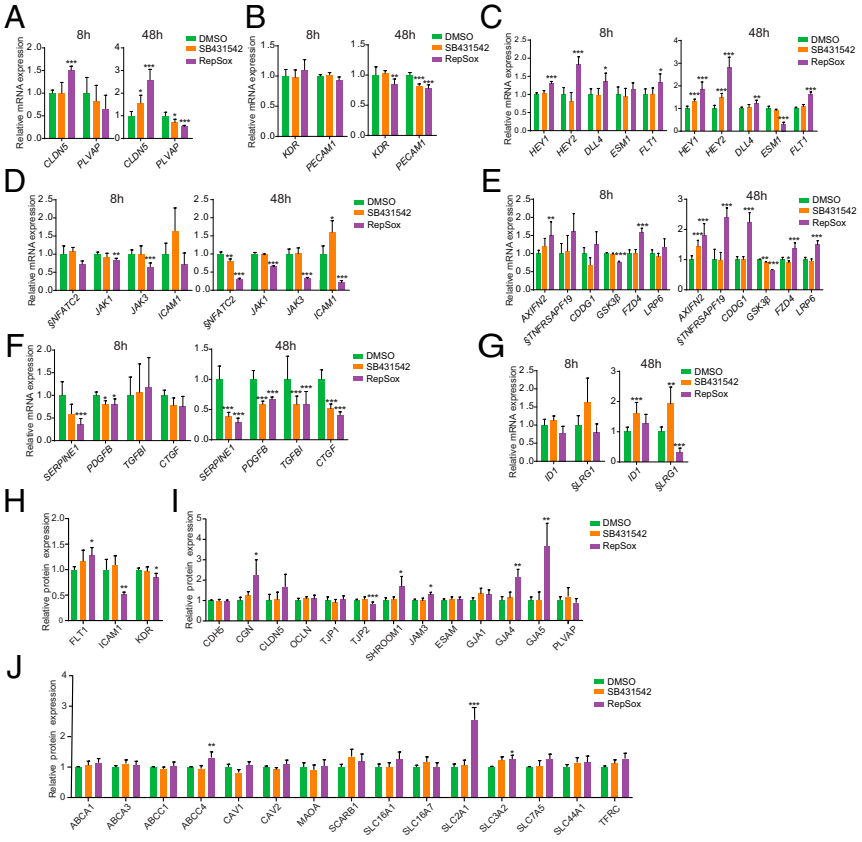

Fig. 6. Molecular evaluation of expression of barrier integrity-related molecules after treatment with RepSox and SB431542. (*A*–*G*) RNA-seq analysis after 8 or 48 h of treatment with TGF-β pathway inhibitors (SB431542 and RepSox) for (*A*) *CLDN5* and *PLVAP*, (*B*) EC markers (*KDR* and *PECAM1*), (*C*) Sprouting/Notch genes (HEY1, HEY2, DLL4, ESM1, and FLT1). (*D*) Inflammatory genes (*NFATC2*, *JAK1*, *JAK3*, and *ICAM1*). (*E*) Wnt signaling genes (AXIN2, TNFRSF19, APCDD1, GSK3β, FZD4, LRP6). (*F*) TGFBR1 signaling genes (*ALK5*, *SERPINE1*, *PDGFB*, *TGFBI*, and *CTGF*) and (*G*) ALK1 signaling genes (*ID1*, and *LRG1*). (*H*–*J*) Mass spectrometry analysis with TGF-β pathway inhibitors (SB431542 and RepSox) for (*H*) inflammatory response-related proteins (FLT1, ICAM1, and KDR), and for (*I*) endothelial barrier-related proteins (CDH5, CGN, CLDN5, OCLN, TJP1, TJP2, SHROOM1, JAM3, ESAM, GJA1, GJA4, GJA5, and PLVAP). Also for (*J*) the BRB/BBB transporter-related proteins (ABCA1, ABCA3, ABCC1, ABCC4, CAV1, CAV2, MAOA, SCARB1, SLC16A1, SLC16A7, GLUT1 [SLC2A1], SLC3A2, SLC7A5, SLC44A1, and TFRC). §, The low RPKM average values for NFATC2, TNFRSF19, and LRG1 (average RPKM < 1) (Dataset S15). Columns are means ± SD. *FDR <0.05, **FDR < 0.01, ***FDR < 0.001.

measured on the EC monolayer, and not a mixture of cells forming the neurovascular junction. Therefore, we detected TEER that is much lower than previously published CNS models (14, 15) but is comparable to the recently published model of ECs monolayer model of CNS-ECs (48). RepSox improved endothelial cells barrier by stimulating expression of tight junction proteins (Claudin-5, ZO-1, and Occludin) in the cell junctions (VE-Cadherin$^+$ area), and by limiting transcytosis in a Caveolin-1–independent manner as observed in CNS-ECs (49).

RepSox has been reported to be a specific inhibitor of TGFBR1 (ALK5) previously (50), but our data suggest that it is a very potent inhibitor of several TGF-β kinase receptors, as well as other kinases. Moreover, by using RNA-seq and mass spectrometry, we identified that RepSox strongly inhibited several other pathways in addition to the TGF-β signaling, suggesting that inhibition of more than one signaling pathway may be required to modulate the EC barrier stability.

Work from others and our labs show that TGF-β signaling is critical for vascular development in vivo. Blood vessels develop in mutant TGFB1 or TGFBR1/2 mice, but the animals die due to intracerebral hemorrhages (51, 52). We showed that RepSox treatments induce dose-dependent vascular remodeling defects. These data suggest that RepSox may inhibit proliferation of vascular stalk cells during angiogenesis. Although RepSox shows as well inhibition of KDR (VEGFR2) and vascular defects could be attributed to KDR inhibition, yet K_d for KDR is in the micromolar range in the kinase competition assay. Therefore, we rather think that the effects are mediated by inhibition of TGFBRs and not VEGFA (53, 54). This is in agreement with a study where TGFBR2 was deleted in the vasculature of developing retina and resulted in vasculature abundant with microaneurysms, leaky capillaries, and retinal hemorrhages (55). On the other hand, several reports (56–58) show that TGF-β signaling is involved in promoting neovascular age-related macular degeneration (nAMD). Therefore, we injected RepSox in rats, as a prophylactic treatment for laser-induced choroidal neovascularization in rats, but observed no RepSox-mediated rescue in the CNV lesion area. There are two possible explanations: 1) Laser photocoagulation damage causes a strong VEGFA response (59), which RepSox is not able to overcome; and 2) timing of the treatment as TGF-β seems to be in the early steps of nAMD antiangiogenic (60–62) possibly as a prosurvival factor for pericytes (63) and through stabilizing the pericyte–EC interaction (64, 65) while, in the late stages of nAMD, TGF-β seems to be proangiogenic (56, 58).

Tight regulation of TGF-β signaling between ECs and vascular smooth muscle cell (SMC)/pericytes is needed to form a mature vascular network (47). This is achieved by synergistic or antagonistic signaling of the receptors such as ALK1 (66), ALK5 (67), endoglin (68), LRG1 (69), and SMOC1 (70) that are expressed on ECs or/and SMCs. This balance is disrupted in pathological settings where, depending on the context, either inhibition or induction of TGF-β signaling can be beneficial. Due to RepSox's broad mechanism of action and our focus on ECs in this study, we foresee that further research is warranted to resolve this controversy.

Collectively, our data suggest that CNS-EC modeling can be enhanced by treating naive EC cultures with RepSox, and that treatment of diseases that result from EC barrier pathologies, such as diabetic retinopathy, Alzheimer's disease, and neuroinflammatory disorders such as multiple sclerosis, as well as psychiatric disorders including depression and schizophrenia, may benefit from therapies targeting more than one signaling pathway simultaneously. Exploring these therapeutic options may improve patient outcomes, and working with more relevant CNS-EC models may improve our understanding of vascular and neuronal homeostasis.

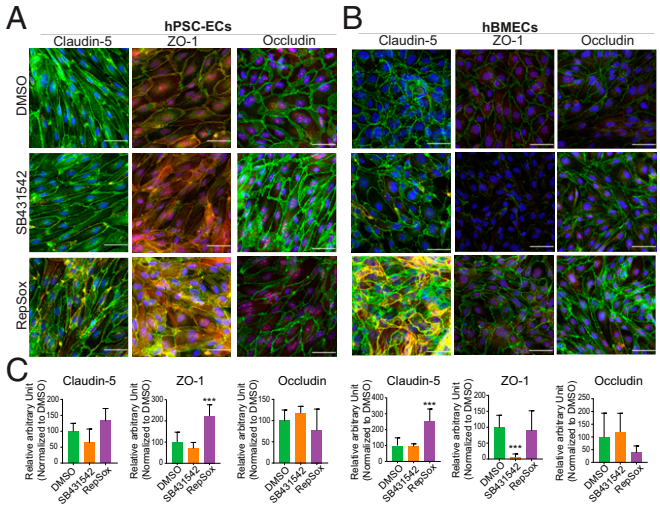

Fig. 7. Confocal imaging of the tight junction proteins treated with DMSO, SB431542, or RepSox. The immunocytochemistry images for each tight junction proteins in (*A*) hPSC-ECs and (*B*) hBMECs. The proteins Claudin-5, ZO-1, and Occludin in red channel, and VE-Cadherin in green, and DAPI in blue. (*C*) The respective quantification of the fluorescence intensity of the individual proteins (Claudin-5, ZO-1, and Occludin) in the area of interest where Claudin-5, ZO-1, or Occludin signal colocalized with VE-Cadherin. Columns are means ± SD. (Scale bars: 50 μm.) The imaging was performed with at least three replicates. ***$P < 0.001$.

Materials and Methods

hPSC Culture and Differentiation. The human ESC line SA001 was obtained from Cellartis AB (71) and routinely screened for mycoplasma contamination. Cells were passaged using Accutase (StemCell Technologies) and replated as small clumps of cells at a dilution of 1:10 to 1:15. For differentiation, hPSCs were dissociated using Accutase. The protocol for differentiation to ECs was described previously (17) with some modifications as follows: Expansion medium, consisting of StemPro with 50 ng/mL VEGFA, was kept on cells only for the first division, and, from the second division, cells were cultured using VascuLife VEGF Endothelial Medium Complete Kit (LifeLine Cell Technology). The final composition of the supplements added to the media was as follows: 10% fetal bovine serum, 4 mM L-glutamine, 0.75 U/mL heparin sulfate, 5 ng/mL fibroblast growth factor-2, 5 ng/mL epidermal growth factor (EGF), 5 ng/mL VEGFA, 15 ng/mL insulin-like growth factor-1, 1 μg/mL hydrocortisone hemisuccinate, and 50 μg/mL ascorbic acid. SB431542 (10 μM) was supplemented when described. The media was changed every other day. Experiments were performed with cells from passages 3 to 9. The SA001 cell line was tested before and after insertion of CLDN5-P2A-GFP using short tandem repeat analysis, G-banding, and an Illumina SNP array (Omni Express) for genetic abnormalities.

Construction of the SPARK Library. A schematic of the SPARK library construction is shown in Fig. 3*A*. Compound, assay, and target information was retrieved from the ChEMBL database (24, 72), version 20 and the internal database of F. Hoffmann-La Roche Ltd., and the two data sources were harmonized using custom scripts. Quantitative activity information derived from dose–response data was used to construct the CAT database, which contains triplets of compounds (indexed by standard InChI keys) (73), activities (quantified by *pAct*, absolute $\log_{10}$ transformed activity values), and molecular targets [indexed by UniProt (25) identifiers and Entrez GeneIDs (26)]. From the ChEMBL database, only data were considered that originated from the scientific literature and reported dose–response bioactivity data as K_i, K_d, IC_{50}, or EC_{50} with a high confidence for the molecular target (ChEMBL confidence score ≥4). If there were multiple activity measurements for the same pair of target and compound, the arithmetic mean of *pAct* values was calculated. Representative compounds that selectively and potently target the druggable genome were chosen using an unsupervised learning approach and clustered based on target profiles using the affinity propagation (AP) clustering method (27) (parameters: q = NA, maxits = 5,000, convits = 500, seed = 1,887; only compounds with two or more targets were considered). To determine the specificity of each compound, the Gini Index (18, 28) was calculated for each compound using *pAct* values of individual genes for which the compound has reported activities. Compounds in each cluster that possess either the highest Gini Index or the highest *pAct* values against each of the genes were chosen for inclusion in the library. When compounds from more than one cluster targeted the same gene, all compounds were included. Next, by manual curation, compounds were removed that were either flagged as potential (pan-assay interference compounds [PAINS]) (74), were not available to us, or have undesirable chemical properties, such as chemically and/or metabolically unstable moieties that may compromise the interpretation of the results as suggested by Blagg and Workman (75). When a compound was removed from the collection, it was replaced with a compound with the similar target profile from the same cluster whenever possible. Lastly, a set of control compounds that were extensively tested against many more target genes than the rest of the compounds were included. To maximize the information available for each of the SPARK compounds, we collected target information by using the CAT database and the proprietary Clarivate Analytics Integrity database. After combining the two data sources, we were able to map the SPARK compounds onto 1,466 unique human genes, each of which is targeted by at least one compound with activity equal or lower to 1 μM. The 1,466 target genes were mapped to 193 distinct UniProt keywords (Dataset S8), which are preferable to those of other classification systems in that target genes are mapped to one or more tags rather than being limited to just one class. By applying the heuristic fuzzy partitioning algorithm developed by the Database for Annotation, Visualization and Integrated Discovery (DAVID) team (76) (with default parameters), 24 target classes uniquely defined by a set of UniProt keywords were identified. UniProt keywords are not mutually exclusive; many of the terms apply to more than one gene (Dataset S8), which better reflects the multiple functions of most drug targets (and more generally, proteins).

To map the SPARK compounds to human pathways and biological processes, the target genes were annotated with terms from the GO BP (31), Reactome pathways (29), and KEGG pathways (30). The same AP clustering algorithm described above was applied, and we found that the GO BP and pathway annotations could be classified into 142 pathway clusters, each of which contained one or more GO BP terms and/or Reactome or KEGG pathways (Dataset S9). The pathway clusters were manually annotated with one of the 16 top-level pathways ("Pathway Category") following the hierarchical structure of the Reactome database (Fig. 3*F*).

SPARK Compound Library Screening Using a Fluorescence-Activated Cell Readout. Compounds were tested in replicate plates with DMSO controls. ECs (10,000 cells per well) were seeded on fibronectin-coated plates containing

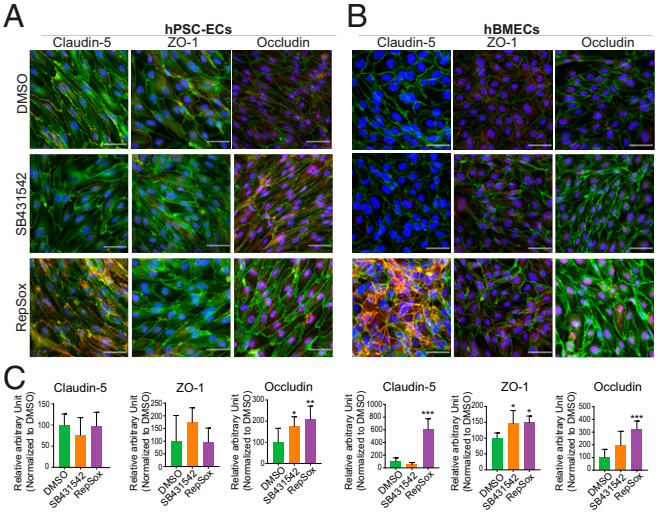

Fig. 8. Confocal imaging of the tight junction proteins cotreated with VEGFA and DMSO, SB431542, or RepSox. The immunocytochemistry images for each tight junction proteins with cotreatment of compounds and VEGFA in (*A*) hPSC-ECs and (*B*) hBMECs. The proteins Claudin-5, ZO-1, and Occludin in red channel, and VE-Cadherin in green, and DAPI in blue. (*C*) The respective quantification of the fluorescence intensity of the individual proteins (Claudin-5, ZO-1, and Occludin) in the area of interest where Claudin-5, ZO-1, or Occludin signal colocalized with VE-Cadherin as the area of interest. Images shown are representative image set with magnification at 20×. Columns are means ± SD. (Scale bars: 50 μm.) The imaging was performed with at least three replicates. *$P < 0.05$, **$P < 0.01$, ***$P < 0.001$.

full media. Cells were treated 48 h after seeding and subjected to FACS analysis on a MACSQuant Analyzer 10 (Miltenyi Biotec) 48 h post-compound treatment. Data were analyzed using the FlowJo V10 software.

ECIS. Endothelial barrier function was detected in real-time using the ECIS Z-theta system (77) (Applied Biophysics) using a 96-well array format (Applied Biophysics) at 250 Hz frequency. Plates were coated with fibronectin (100 μL of 25 μg/mL) for 30 min at room temperature, which was then replaced with complete media and electrodes and stabilized for 1 h on the system. Afterward, media was removed, and hPSC-ECs were seeded (10,000 cells per well). Cells were grown for 48 h to reach full confluency and were then treated with compounds, with or without VEGFA (50 ng/mL). All treatments were performed in triplicate.

TEER Assay. The TEER values of hPSC-ECs, hBMECs (CellSystem), and hRMECs (PELO Biotech) were measured using the cellZscope (nanoAnalytics, Münster, Germany). Cells were prepared on HTS Transwell-24 Well format (Corning) at 0.4×10^6 cells per square centimeter and we let them grow for 48 h in order to form an even monolayer. Afterward, SB431542 (10 μM) or RepSox (10 μM) or DMSO was added on the apical chamber. The TEER values were recorded in real time every 30 min automatically in triplicate.

Cellular Transcytosis Assay. The hPSC-ECs were plated on fibronectin (Corning)-coated cover glass (VWR) at 63,000 cells per square centimeter in a 24-well culture plate. A day after, the cells were treated with DMSO (0.1%) as a vehicle control, 10 μM SB431542, and 10 μM RepSox. Then, after 48 h incubation with compounds, the hPSC-ECs were treated with CtxB, Alexa Fluor 647 Conjugate (Thermo) at 5 μg/mL per well. After a 30 min incubation at 37 °C in a humidified chamber, the cells were fixed with 4% paraformaldehyde and rinsed with phosphate-buffered saline three times. The fixed cells on the coverslips were stained with Caveolin-1 (3238; 1:200; CellSignaling) and mounted with Fluorescence Mounting Medium (DAKO) including DAPI for confocal imaging.

Statistical Analysis. Prism 7 (GraphPad) was used to create charts and perform statistical analyses. Statistical analysis included unpaired, two-tailed Student's *t* test, unless mentioned otherwise. For all bar graphs, data are represented as mean ± SD. *P* values <0.05 were considered significant.

ACKNOWLEDGMENTS. We thank Martine Kapps, Nicole Soder, and Silke Zimmerman for technical assistance. This study was supported by F. Hoffmann-La Roche Ltd. F. Roudnicky, N.J.P., and V.K. were supported by a Roche postdoctoral fellowship. B.K.K. was supported by a Roche doctoral fellowship.

1. B. Engelhardt, S. Liebner, Novel insights into the development and maintenance of the blood-brain barrier. *Cell Tissue Res.* **355**, 687–699 (2014).
2. M. Díaz-Coránguez, C. Ramos, D. A. Antonetti, The inner blood-retinal barrier: Cellular basis and development. *Vision Res.* **139**, 123–137 (2017).
3. I. Klaassen, C. J. Van Noorden, R. O. Schlingemann, Molecular basis of the inner blood-retinal barrier and its breakdown in diabetic macular edema and other pathological conditions. *Prog. Retin. Eye Res.* **34**, 19–48 (2013).
4. Z. Zhao, A. R. Nelson, C. Betsholtz, B. V. Zlokovic, Establishment and dysfunction of the blood-brain barrier. *Cell* **163**, 1064–1078 (2015).
5. A. C. Luissint, C. Artus, F. Glacial, K. Ganeshamoorthy, P. O. Couraud, Tight junctions at the blood brain barrier: Physiological architecture and disease-associated dysregulation. *Fluids Barriers CNS* **9**, 23 (2012).
6. C. Greene, N. Hanley, M. Campbell, Claudin-5: Gatekeeper of neurological function. *Fluids Barriers CNS* **16**, 3 (2019).
7. Y. Zhang *et al*., An RNA-sequencing transcriptome and splicing database of glia, neurons, and vascular cells of the cerebral cortex. *J. Neurosci.* **34**, 11929–11947 (2014).
8. M. Vanlandewijck *et al*., A molecular atlas of cell types and zonation in the brain vasculature. *Nature* **554**, 475–480 (2018).
9. T. Nitta *et al*., Size-selective loosening of the blood-brain barrier in claudin-5-deficient mice. *J. Cell Biol.* **161**, 653–660 (2003).
10. M. Campbell *et al*., Targeted suppression of claudin-5 decreases cerebral oedema and improves cognitive outcome following traumatic brain injury. *Nat. Commun.* **3**, 849 (2012).
11. C. Greene *et al*., Dose-dependent expression of claudin-5 is a modifying factor in schizophrenia. *Mol. Psychiatry* **23**, 2156–2166 (2018).
12. D. Bouïs, G. A. Hospers, C. Meijer, G. Molema, N. H. Mulder, Endothelium in vitro: A review of human vascular endothelial cell lines for blood vessel-related research. *Angiogenesis* **4**, 91–102 (2001).
13. Z. Zhu, D. Huangfu, Human pluripotent stem cells: An emerging model in developmental biology. *Development* **140**, 705–717 (2013).
14. E. S. Lippmann *et al*., Derivation of blood-brain barrier endothelial cells from human pluripotent stem cells. *Nat. Biotechnol.* **30**, 783–791 (2012).
15. S. G. Canfield *et al*., An isogenic blood-brain barrier model comprising brain endothelial cells, astrocytes, and neurons derived from human induced pluripotent stem cells. *J. Neurochem.* **140**, 874–888 (2017).
16. K. Christensen, F. Roudnicky, M. Burcin, C. Patsch, Monolayer generation of vascular endothelial cells from human pluripotent stem cells. *Methods Mol. Biol.* **1994**, 17–29 (2019).
17. C. Patsch *et al*., Generation of vascular endothelial and smooth muscle cells from human pluripotent stem cells. *Nat. Cell Biol.* **17**, 994–1003 (2015).
18. J. D. Zhang *et al*., Detect tissue heterogeneity in gene expression data with BioQC. *BMC Genomics* **18**, 277 (2017).
19. A. R. R. Forrest *et al*.; FANTOM Consortium and the RIKEN PMI and CLST (DGT), A promoter-level mammalian expression atlas. *Nature* **507**, 462–470 (2014).
20. A. Liberzon *et al*., The Molecular Signatures Database (MSigDB) hallmark gene set collection. *Cell Syst.* **1**, 417–425 (2015).
21. D. W. Leung, G. Cachianes, W. J. Kuang, D. V. Goeddel, N. Ferrara, Vascular endothelial growth factor is a secreted angiogenic mitogen. *Science* **246**, 1306–1309 (1989).
22. D. R. Senger *et al*., Tumor cells secrete a vascular permeability factor that promotes accumulation of ascites fluid. *Science* **219**, 983–985 (1983).
23. D. B. Mendel *et al*., In vivo antitumor activity of SU11248, a novel tyrosine kinase inhibitor targeting vascular endothelial growth factor and platelet-derived growth factor receptors: Determination of a pharmacokinetic/pharmacodynamic relationship. *Clin. Cancer Res.* **9**, 327–337 (2003).
24. A. Gaulton *et al*., ChEMBL: A large-scale bioactivity database for drug discovery. *Nucleic Acids Res.* **40**, D1100–D1107 (2012).
25. T. UniProt Consortium, UniProt: The universal protein knowledgebase. *Nucleic Acids Res.* **46**, 2699 (2018).
26. D. Maglott, J. Ostell, K. D. Pruitt, T. Tatusova, Entrez gene: Gene-centered information at NCBI. *Nucleic Acids Res.* **33** (suppl. 1), D54–D58 (2005).
27. B. J. Frey, D. Dueck, Clustering by passing messages between data points. *Science* **315**, 972–976 (2007).
28. L. Ceriani, P. Verme, The origins of the Gini index: Extracts from Variabilità e Mutabilità (1912) by Corrado Gini. *J. Econ. Inequal.* **10**, 421–443 (2012).
29. A. Fabregat *et al*., The reactome pathway knowledgebase. *Nucleic Acids Res.* **46**, D649–D655 (2018).
30. H. Ogata *et al*., KEGG: Kyoto Encyclopedia of Genes and Genomes. *Nucleic Acids Res.* **27**, 29–34 (1999).
31. M. Ashburner *et al*.; The Gene Ontology Consortium, Gene ontology: Tool for the unification of biology. *Nat. Genet.* **25**, 25–29 (2000).
32. A. T. Argaw, B. T. Gurfein, Y. Zhang, A. Zameer, G. R. John, VEGF-mediated disruption of endothelial CLN-5 promotes blood-brain barrier breakdown. *Proc. Natl. Acad. Sci. U.S.A.* **106**, 1977–1982 (2009).
33. L. A. Strickland *et al*., Plasmalemmal vesicle-associated protein (PLVAP) is expressed by tumour endothelium and is upregulated by vascular endothelial growth factor-A (VEGF). *J. Pathol.* **206**, 466–475 (2005).
34. F. Roudnicky *et al*., Endocan is upregulated on tumor vessels in invasive bladder cancer where it mediates VEGF-A-induced angiogenesis. *Cancer Res.* **73**, 1097–1106 (2013).
35. S. W. Lukowski *et al*., Single-cell transcriptional profiling of aortic endothelium identifies a hierarchy from endovascular progenitors to differentiated cells. *Cell Rep.* **27**, 2748–2758.e3 (2019).
36. I. R. McCracken *et al*., Transcriptional dynamics of pluripotent stem cell-derived endothelial cell differentiation revealed by single-cell RNA sequencing. *Eur. Heart J.* **41**, 1024–1036 (2020).
37. L. Yuan *et al*., ETS-related gene (ERG) controls endothelial cell permeability via transcriptional regulation of the claudin 5 (CLDN5) gene. *J. Biol. Chem.* **287**, 6582–6591 (2012).
38. M. S. Kluger, P. R. Clark, G. Tellides, V. Gerke, J. S. Pober, Claudin-5 controls intercellular barriers of human dermal microvascular but not human umbilical vein endothelial cells. *Arterioscler. Thromb. Vasc. Biol.* **33**, 489–500 (2013).
39. S. Dandapani, G. Rosse, N. Southall, J. M. Salvino, C. J. Thomas, Selecting, acquiring, and using small molecule libraries for high-throughput screening. *Curr. Protoc. Chem. Biol.* **4**, 177–191 (2012).
40. S. M. Corsello *et al*., The drug repurposing hub: A next-generation drug library and information resource. *Nat. Med.* **23**, 405–408 (2017).
41. C. H. Arrowsmith *et al*., The promise and peril of chemical probes. *Nat. Chem. Biol.* **11**, 536–541 (2015). Erratum in: *Nat. Chem. Biol.* **11**, 887 (2015).
42. A. A. Antolin *et al*., Objective, quantitative, data-driven assessment of chemical probes. *Cell Chem. Biol.* **25**, 194–205.e5 (2018).
43. Y. Wang *et al*., Evidence-based and quantitative prioritization of tool compounds in phenotypic drug discovery. *Cell Chem. Biol.* **23**, 862–874 (2016).
44. N. Moret *et al*., Cheminformatics tools for analyzing and designing optimized small-molecule collections and libraries. *Cell Chem. Biol.* **26**, 765–777.e3 (2019).
45. T. Watabe *et al*., TGF-beta receptor kinase inhibitor enhances growth and integrity of embryonic stem cell-derived endothelial cells. *J. Cell Biol.* **163**, 1303–1311 (2003).

46. N. Rudini *et al*., VE-cadherin is a critical endothelial regulator of TGF-beta signalling. *EMBO J.* **27**, 993–1004 (2008).
47. M. J. Goumans, Z. Liu, P. ten Dijke, TGF-beta signaling in vascular biology and dysfunction. *Cell Res.* **19**, 116–127 (2009).
48. C. Praça *et al*., Derivation of brain capillary-like endothelial cells from human pluripotent stem cell-derived endothelial progenitor cells. *Stem Cell Reports* **13**, 599–611 (2019).
49. S. Ayloo, C. Gu, Transcytosis at the blood-brain barrier. *Curr. Opin. Neurobiol.* **57**, 32–38 (2019).
50. F. Gellibert *et al*., Identification of 1,5-naphthyridine derivatives as a novel series of potent and selective TGF-β type I receptor inhibitors. *J. Med. Chem.* **47**, 4494–4506 (2004).
51. M. A. McMillin *et al*., TGFβ1 exacerbates blood-brain barrier permeability in a mouse model of hepatic encephalopathy via upregulation of MMP9 and downregulation of claudin-5. *Lab. Invest.* **95**, 903–913 (2015).
52. M. A. Behzadian, X. L. Wang, L. J. Windsor, N. Ghaly, R. B. Caldwell, TGF-beta increases retinal endothelial cell permeability by increasing MMP-9: Possible role of glial cells in endothelial barrier function. *Invest. Ophthalmol. Vis. Sci.* **42**, 853–859 (2001).
53. S. K. Halder, R. D. Beauchamp, P. K. Datta, A specific inhibitor of TGF-beta receptor kinase, SB-431542, as a potent antitumor agent for human cancers. *Neoplasia* **7**, 509–521 (2005).
54. M. Zhang *et al*., Blockade of TGF-β signaling by the TGFβR-I kinase inhibitor LY2109761 enhances radiation response and prolongs survival in glioblastoma. *Cancer Res.* **71**, 7155–7167 (2011).
55. B. M. Braunger *et al*., Deletion of ocular transforming growth factor β signaling mimics essential characteristics of diabetic retinopathy. *Am. J. Pathol.* **185**, 1749–1768 (2015).
56. X. Wang *et al*., TGF-β participates choroid neovascularization through Smad2/3-VEGF/TNF-α signaling in mice with Laser-induced wet age-related macular degeneration. *Sci. Rep.* **7**, 9672 (2017).
57. N. Ogata *et al*., Expression of transforming growth factor-beta mRNA in experimental choroidal neovascularization. *Curr. Eye Res.* **16**, 9–18 (1997).
58. S. Recalde *et al*., Transforming growth factor-β inhibition decreases diode laser-induced choroidal neovascularization development in rats: P17 and P144 peptides. *Invest. Ophthalmol. Vis. Sci.* **52**, 7090–7097 (2011).
59. N. Kwak, N. Okamoto, J. M. Wood, P. A. Campochiaro, VEGF is major stimulator in model of choroidal neovascularization. *Invest. Ophthalmol. Vis. Sci.* **41**, 3158–3164 (2000).
60. G. M. Tosi, M. Orlandini, F. Galvagni, The controversial role of TGF-β in neovascular age-related macular degeneration pathogenesis. *Int. J. Mol. Sci.* **19**, E3363 (2018).
61. C. B. M. Platania *et al*., Topical ocular delivery of TGF-β1 to the back of the eye: Implications in age-related neurodegenerative diseases. *Int. J. Mol. Sci.* **18**, E2076 (2017).
62. A. Schlecht *et al*., Deletion of endothelial transforming growth factor-β signaling leads to choroidal neovascularization. *Am. J. Pathol.* **187**, 2570–2589 (2017).
63. S.-C. Shih *et al*., Transforming growth factor beta1 induction of vascular endothelial growth factor receptor 1: Mechanism of pericyte-induced vascular survival in vivo. *Proc. Natl. Acad. Sci. U.S.A.* **100**, 15859–15864 (2003).
64. T. E. Walshe *et al*., TGF-β is required for vascular barrier function, endothelial survival and homeostasis of the adult microvasculature. *PLoS One* **4**, e5149 (2009).
65. K. K. Hirschi, S. A. Rohovsky, P. A. D'Amore, PDGF, TGF-β, and heterotypic cell-cell interactions mediate endothelial cell-induced recruitment of 10T1/2 cells and their differentiation to a smooth muscle fate. *J. Cell Biol.* **141**, 805–814 (1998).
66. S. P. Oh *et al*., Activin receptor-like kinase 1 modulates transforming growth factor-beta 1 signaling in the regulation of angiogenesis. *Proc. Natl. Acad. Sci. U.S.A.* **97**, 2626–2631 (2000).
67. M. J. Goumans *et al*., Activin receptor-like kinase (ALK)1 is an antagonistic mediator of lateral TGFbeta/ALK5 signaling. *Mol. Cell* **12**, 817–828 (2003).
68. F. Lebrin *et al*., Endoglin promotes endothelial cell proliferation and TGF-beta/ALK1 signal transduction. *EMBO J.* **23**, 4018–4028 (2004).
69. X. Wang *et al*., LRG1 promotes angiogenesis by modulating endothelial TGF-β signalling. *Nature* **499**, 306–311 (2013).
70. K. Awwad *et al*., Role of secreted modular calcium-binding protein 1 (SMOC1) in transforming growth factor β signalling and angiogenesis. *Cardiovasc. Res.* **106**, 284–294 (2015).
71. M. C. Englund *et al*., The establishment of 20 different human embryonic stem cell lines and subclones; a report on derivation, culture, characterisation and banking. *In Vitro Cell. Dev. Biol. Anim.* **46**, 217–230 (2010).
72. A. Gaulton *et al*., The ChEMBL database in 2017. *Nucleic Acids Res.* **45**, D945–D954 (2017).
73. S. R. Heller, A. McNaught, I. Pletnev, S. Stein, D. Tchekhovskoi, InChI, the IUPAC international chemical identifier. *J. Cheminform.* **7**, 23 (2015).
74. J. B. Baell, G. A. Holloway, New substructure filters for removal of pan assay interference compounds (PAINS) from screening libraries and for their exclusion in bioassays. *J. Med. Chem.* **53**, 2719–2740 (2010).
75. J. Blagg, P. Workman, Choose and use your chemical probe wisely to explore cancer biology. *Cancer Cell* **32**, 268–270 (2017).
76. D. W. Huang *et al*., The DAVID Gene Functional Classification Tool: A novel biological module-centric algorithm to functionally analyze large gene lists. *Genome Biol.* **8**, R183 (2007).
77. M. J. Bernas *et al*., Establishment of primary cultures of human brain microvascular endothelial cells to provide an in vitro cellular model of the blood-brain barrier. *Nat. Protoc.* **5**, 1265–1272 (2010).